Towards Practical Sulfolane Based Electrolytes: Choice of Li salt for Graphite Electrode Operation

Tong Zhang[1], Willy Porcher[2], Elie Paillard[1*]

[1]*Helmholtz Institute Münster – Forschungszentrum Jülich (IEK-12), Correnstrasse 80, 48149 Münster, Germany*

[2] *Université Grenoble Alpes, CEA-Liten, 17 rue des Martyrs, F-38054 Grenoble, France*

Abstract:

Sulfolane (tetramethylene sulfone, SL) is known for leading to Li-ion electrolytes with high anodic stability. However, the operation of graphite electrodes in alternative electrolytes is usually challenging, especially when ethylene carbonate (EC) is not used as co-solvent. Thus, we study here the influence of the lithium salt on the physico-chemical and electrochemical properties of EC-free SL-based electrolytes and on the performance of graphite electrodes based on carboxymethyl cellulose (CMC). SL mixed with dimethyl carbonate (DMC) leads to electrolytes as conductive as state-of-the-art alkyl carbonate-based electrolytes with wide electrochemical stability windows. The compatibility with graphite electrodes depends on the Li salt used and, even though cycling is possible with most salts, lithium difluoro-oxalato borate (LiDFOB) is especially interesting for graphite operation. LiDFOB electrolytes are conductive at room temperature (*ca.* 6 mS cm^{-1}) with an anodic stability slightly below 5 V vs. Li/Li^+ on particulate carbon black electrodes. In addition, it allows cycling graphite electrodes with steady capacity and high coulombic efficiency without any additive. The testing of graphite electrodes in half-cells is, however, problematic with SL:DMC mixtures and, by switching the Li metal counter electrode for $LiFePO_4$, the graphite electrode achieves better practical performance in terms of rate capability.

Keywords: Sulfolane, Electrolyte, Lithium-ion, graphite, LiFSI, LiTDI, LiDFOB

* Corresponding author: e.paillard@fz-juelich.de

1. Introduction

Current lithium-ion batteries (LIBs) electrolytes are mostly made of lithium hexafluorophosphate ($LiPF_6$) dissolved in mixtures of ethylene carbonate (EC) and linear alkyl carbonates such as dimethyl carbonate (DMC), diethyl carbonate (DEC) or ethylmethyl carbonate (EMC) [1–3]. The use of EC was once dictated by the use of graphite electrodes, for which EC possesses excellent Solid Electrolyte Interphase (SEI) [4,5] forming ability. More recently, SEI additives, such as vinylene carbonate (VC) or fluoroethylene carbonate (FEC) have allowed the operation of graphite anodes even when mixed with electrolytes with poor SEI forming ability such as propylene carbonate (PC) [6], alklynitriles [7], linear sulfones [8] or TFSI-based ionic liquids [9]. However, for best graphite performance, mixtures of EC and linear alkyl carbonates are still mainly used, in combination with additives.

In the last years, many attempts have been made to increase further the energy density of LIBs and cathode materials operating above 4.5 V versus Li/Li^+ have been proposed in the late 90's, such as $LiNi_{0.5}Mn_{1.5}O_4$ [10,11], $LiCoPO_4$ [12,13] or, more recently, $LiCoPO_4F$ [14,15]. However, the so-called '5 V' LIB is still not a reality, due to the failure of EC/linear alkyl carbonate mixtures to operate above 4.3 V. Indeed, if the electronic structure (HOMO) of each single electrolyte components plays a role in the anodic stability of electrolyte mixtures [16], the presence of Li salt [17] often leads to inferior anodic stabilities than those derived from HOMO calculation for the solvent alone. In particular, it explains why EC, despite having among the lowest calculated HOMO energy of all alkyl carbonate solvents, leads to electrolytes with lower practical anodic stabilities as compared to it intrinsic stability. In fact, Borodin *et al*. noted the detrimental effects of BF_4, PF_6 and $B(CN)_4$ on alkyl carbonate solvents, while, on the other hand, they have less influence of sulfone-based solvents such as sulfolane (SL) (Figure 1a), which explains their better performance at high voltage [18,19]. According to these studies, however, DMC anodic stability was found to be also significantly lowered by the presence of Li salts, whereas mixtures of SL and other solvents, such as EMC [20] or ethyl acetate [21] are reported having similar anodic stability as SL alone. The reason would be linked to the double layer structure where the electro-oxidation occurs [22], which also explains the stronger decomposition of EC vs. DMC in EC/DMC mixtures [23].

SL is a by-product of the oil industry, thus cheap and produced by tons [24]. Its high potential of

oxidation, as well as those of linear sulfones [25], above 5 V vs. Li/Li^+ has recently attracted interest as a high voltage electrolyte solvent [26]. Moreover, concerning the practical stability in reduction (linked to the ability to form an effective SEI onto graphite and Li metal electrodes), SL was used as early as 1985 in Li metal studies [27] and a first report of a *'high EMF'* electrochemical cell based on Li metal electrodeposited onto graphite from SL electrolytes was issued in 1971 [28]. More recently, SL has shown promising SEI forming ability on graphite at 90 °C [29], which makes it a good candidate for Li-ion application, while linear alkyl sulfones necessitate SEI forming additives for graphite operation [8].

Despite these interesting properties and studies focusing on cathodes performance [30,31], only few reports deal with carbon-based electrodes [32] and even less [33] with EC-free electrolytes able to operate a full Li-ion cell including graphite. Recently, Dahn's group reported on full Li-ion using VC and other additives in SL-based electrolytes [34] and we reported that, by use of carboxymethyl cellulose (CMC)/styrene-butadiene rubber (SBR)-based graphite anodes, efficient cycling of graphite is possible in a 1 M $LiPF_6$ SL:DMC (1:1, wt.) electrolyte without any SEI forming additives [35]. As it is known that the Li salt can have a strong influence on the SEI formation on graphite [36–38], we examine here the effect of various lithium salts, (shown in Figure 1a), on the physico-chemical properties of SL:DMC-based electrolytes and assess their suitability for graphite electrode operation.

2. Experimental

Electrolytes: The commercial electrolytes LP30 (1 M $LiPF_6$ EC:DMC (1:1, wt.)) and LP47 (1 M $LiPF_6$ EC:DEC (3:7, wt.)) were purchased from BASF (Selectilyte™), stored in a Mbraun glove box under argon atmosphere with O_2 and H_2O content below 1 ppm and and used as received. The lithium salts were used either as received ($LiBF_4$ (Sigma-Aldrich, 99.99%) and $LiPF_6$ (Sigma-Aldrich, 99.99%)) or after drying under vacuum at 80 °C for 48 h (lithium difluoro(oxalato)borate (LiDFOB) (Sigma-Aldrich) or at 90 °C for 48 h (lithium bis(trifluoromethanesulfonyl)imide (LiTFSI) (3M, 99.99%), lithium bis(fluorosulfonyl)imide (LiFSI) (99%, Provisco CZ), lithium 2-trifluoromethyl-4,5-dicyanoimidazole (LiTDI) (Solvionic, 99%)). DMC (BASF, Selectilyte™) was used as received and SL (Sigma-Aldrich, 99%) was distillated under vacuum and dried with molecular sieves (3A) until the water content decreased below 20 ppm as determined by coulometric Karl-Fischer titration on a KF 851 Titrando (Mettler Toledo) located in a dry room (RH < 0.2% at

20°C). All electrolytes were prepared by mixing the lithium salt with pre-mixed SL:DMC (1:1, wt.) in a Mbraun glove box under argon atmosphere with O_2 and H_2O content below 1 ppm. The final electrolytes all had water content below 40 ppm as determined by Karl-Fisher titration.

Electrodes: Graphite electrode composition: 96/2/2 (graphite (SLP30, Timcal)/CMC/SBR), total mass loading: 7.5 mg cm^{-2}. LFP electrode: 90.5/4.5/5 (LFP/PVdF/Carbon black), total mass loading: 17 mg cm^{-2}. Carbon black electrodes composition: 90/10 (Super C65 (IMERYS)/PVdF (Solef 5130, Solvay)). The active mass loading of the electrodes was *ca.* 1 mg cm^{-2}. Graphite, LFP and carbon black electrodes (12 mm Ø) were punched and dried in vacuum at 110 °C for 48 h. Ni foil (99.99%, Schlenk), previously washed with ethanol, was punched into electrodes (12 mm Ø) and dried in vacuum at 80 °C for 24 h before the electrochemical stability window test. Pt electrodes (1 mm Ø, eDAQ) were polished and washed with acetone and dried under vacuum for 1h before each voltamperometry scan.

Thermal analysis: Differential scanning calorimetry (DSC) was performed on a Q2000 DSC (TA Instrument) under helium flow. Aluminum hermetic (TZERO™) pans were sealed in a glove box with H_2O and O_2 below 1 ppm. The samples were annealed at low temperature to favor crystallization: At 10 °C min^{-1}, a cooling ramp from 20 °C to -150 °C was followed by a heating ramp to -30 °C with a 15 min isotherm and by a ramp down to -150 °C. The final heating ramp to 60 °C was then done at 5 °C min^{-1}.

Viscosity and density: Viscosity and density were measured using a Stabinger Viscometer™ (Anton Paar, SVM™ 3001) located in a dry room (RH < 0.2% at 20 °C).

Electrochemical tests: Linear sweep voltammetries were performed with a VMP3 potentiostat (BioLogic) in three electrode Swagelok™ cells with Li counter and reference electrodes (Rockwood lithium) at room temperature (*ca*. 21-23 °C), using glass fiber separator (Whatmann GF/D), previously dried under vacuum at 200°C for 24 h. Galvanostatic cycling was done on a Maccor 4300 battery cycler in three electrode Swagelok™ cells placed in a temperature-controlled chamber at 20 °C. Conductivity was measured using a BioLogic MCS10, impedance-based conductimeter, from 60 °C to -40 °C with 30 min stabilization every 5 °C, followed by a temperature ramp from -40 °C to 60 °C at the same rate, using hermetical cells sealed in a Mbraun glove box under argon atmosphere with O_2 and H_2O content below 1 ppm.

3. Results and discussion

Six different lithium salts were used to prepare 1 M electrolytes in SL:DMC (1:1, wt.). The salts and solvents and their acronyms are shown in Figure 1a. Their practical temperature ranges (liquid range) were evaluated by DSC. Viscosity, density, and conductivity were measured as well to better understand the respective influence of dissociation and viscosity on the conductivity behavior. The size and molecular weight of the anions are also reported in Table 1, as these parameters likely influence the electrolyte properties.

Liquid range

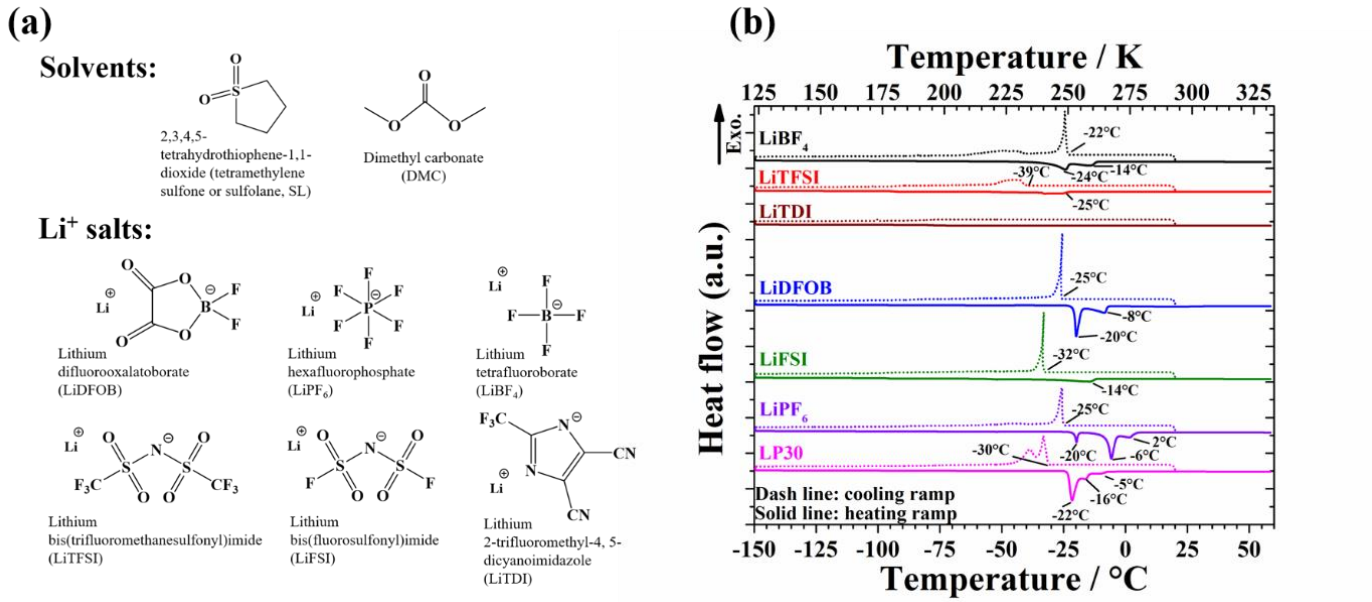

Figure 1. (a) *Structural formulae and acronyms of solvents and lithium salts used,* ***(b)*** *DSC traces of the 1 M SL:DMC (1:1, wt.) electrolytes and LP30. First cooling (10 °C min^{-1}) and last heating (5 °C min^{-1}) ramps shown.*

The DSC traces of the 1 M SL:DMC (1:1, wt.) electrolytes incorporating the lithium salts are shown in Figure 1b and compared with the reference electrolyte LP30 (1 M $LiPF_6$ EC:DMC (1:1, wt.). Excepted for the LiTDI system, all electrolytes crystallize during the first cooling ramp and the crystallization temperatures follows the trend: $LiBF_4$ > LiDFOB = $LiPF_6$ > LP30 > LiFSI > LiTFSI. In these conditions, the reference electrolyte LP30 crystallizes at a slightly lower temperature (-30 °C) as compared with the 1 M $LiPF_6$ SL:DMC electrolyte and only the LiFSI and LiTFSI electrolyte crystallizes at lower temperature. On the

heating ramps, all the electrolytes (except the LiTDI electrolyte) show one or several melting transitions, likely due to the presence of salt/solvent crystalline complexes. The last melting temperatures are in the following order: $LiPF_6$ > LP30 > LiDFOB > $LiBF_4$ = LiFSI > LiTFSI. Therefore, only the $LiPF_6$ electrolyte exhibits a last melting transition above that of the reference electrolyte LP30.

Density, viscosity and conductivity

The variation of densities of the SL:DMC (1:1, wt.) electrolytes are shown in Figure 2a. Overall, the densities are below that of LP30 and increase with the size of the anion, from $LiBF_4$ to $LiPF_6$ and from LiFSI to LiTFSI. LiTDI leads to the lowest measured density despite having, a size similar to that of TFSI and a similar weight as FSI. DFOB also induces a rather low density. TDI and DFOB are rigid anions as both incorporate a planar moiety, whereas FSI [39] and TFSI [40] have high conformational flexibility. It probably results, in addition to their own '*intrinsic'* lower density, in a denser packing around solvated Li^+. In fact, TFSI, in acetonitrile, tends to form mostly solvent separated ion pairs (SSIP) and contact ion pairs (CIP) at mole fractions below 0.1 (which is the case here at 1 M). In SSIPs, Li^+ is coordinated by four solvent molecules and the anion is uncoordinated, for CIPs, by three solvent molecules and one anion that does not interact with other Li^+ [41]. Moreover, LiFSI was found to be even more dissocated [42]. In fact, molecular dynamics simulation found that the probability of forming a solvate incorporating n ions decreases exponentially with n [43]. TDI, on the other hand, interacts by both its –CN groups and the nitrogen atoms on the aromatic ring. Thus, it easily forms polymeric chains between several Li^+ centers bridged by TDI anions. Such structures are found in various LiTDI/solvent crystalline structures [44] and it was found that, in ether mixtures including LiTDI, larger polysulfide clusters are formed as compared with equivalent LiTFSI electrolytes [45]. DFOB, on the other hand, mostly interacts with Li^+ via its carbonyl groups, and only to a lesser extent, via its fluorine atom in the liquid phase and is coordinated similarly to LiTFSI [46].

The variations with temperature are linear and can be fitted with equation 1 and the parameters ρ_0 and a are reported in Table 1.

$$\rho = \rho_0 + aT \qquad \textbf{(1)}$$

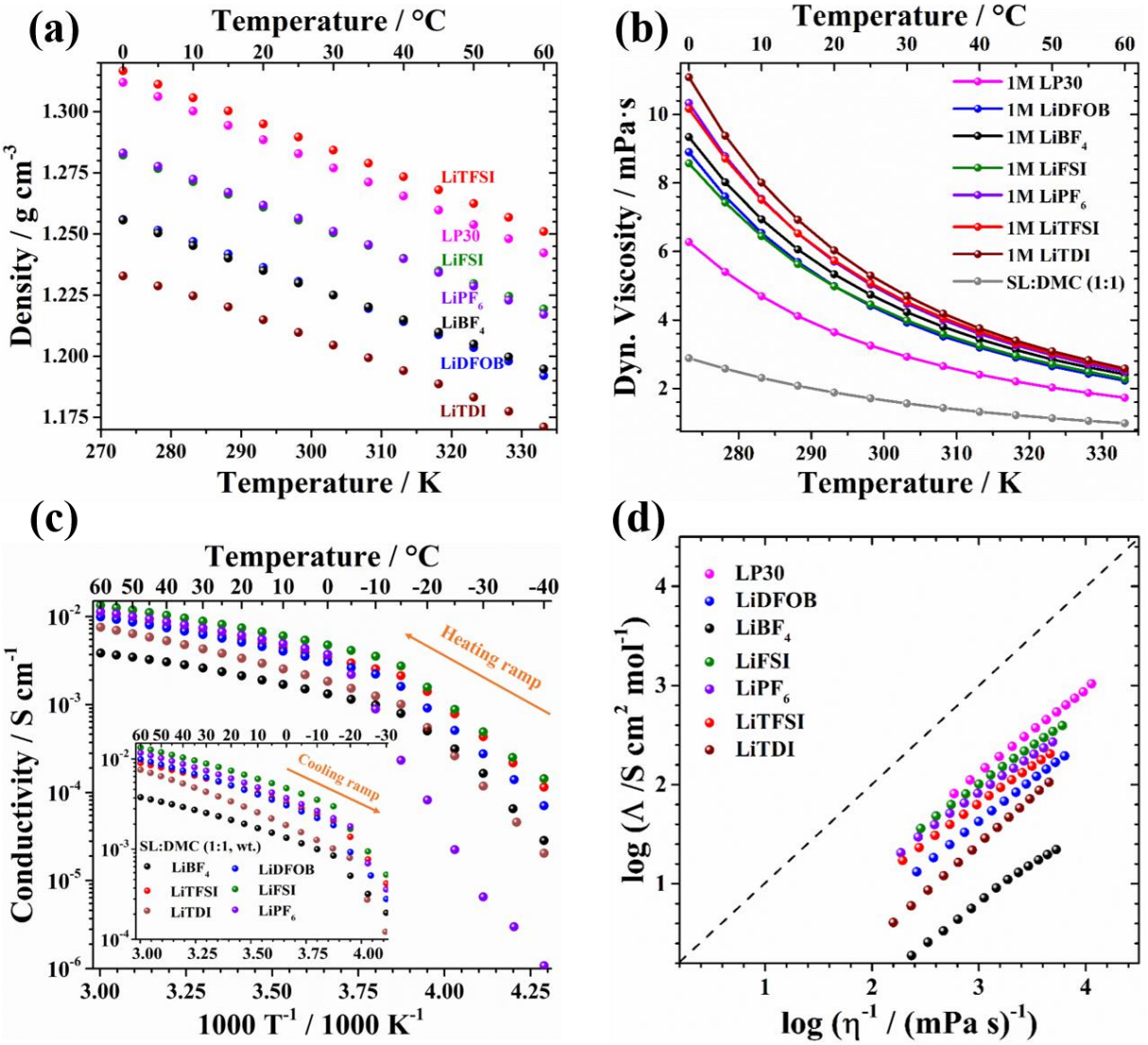

Figure 2. ***(a)*** *Density of the 1 M SL:DMC (1:1, wt.) electrolytes and LP30 as a function of temperature;* ***(b)*** *Viscosities of the 1 M SL:DMC (1:1) electrolytes, LP30 and SL:DMC (1:1, wt.) as a function of temperature;* ***(c)*** *Conductivities of the 1 M SL:DMC (1:1, wt.) electrolytes;* ***(d)*** *Walden plots of the 1 M SL:DMC (1:1, wt.) electrolytes and LP30.*

The viscosity values of SL:DMC (1:1, wt.) and the 1 M electrolytes are reported in Figure 2b with those of LP30. The addition of DMC as co-solvent decreases the viscosity of the SL:DMC binary solvent by a factor 7 as compared with pure SL (at 30 °C, η(SL) = 10.3 mPa s [47]), allowing the viscosities of the 1 M SL:DMC (1:1, wt.) electrolytes to be in same range as LP30, although 30% to 50% higher. The viscosities follow the trend: LiTDI > $LiPF_6$ ≈ LiTFSI > $LiBF_4$ > LiDFOB ≈ LiFSI.

If anion size explains the differences for the salts that lead to smaller solvates structures (i.e. LiFSI, LiTFSI and LiDFOB), the LiTDI electrolyte exhibits a relatively high viscosity which contrasts with a previous report in EC:DMC (1:1) [48]. The high viscosity of the LiTDI electrolyte probably proceeds from the same reasons as the low density of the electrolytes, with a reduced mobility of species due to the presence of larger aggregates. $LiBF_4$ which is usually less dissociated [2], leads to a more viscous electrolyte than the larger LiDFOB and LiFSI salts.

Conductivity

The conductivity values of the 1 M SL:DMC (1:1, wt.) electrolytes are shown in Figure 2c. In the conditions of the measurement, the electrolytes all switch from an Arrhenius (linear part in crystalline or semi-crystalline state) to Vogel Tammann Fulcher (VTF) (curved part, in molten state). The LiTDI electrolyte, which did not crystallize during DSC measurements, also shows a transition, between -20 °C and -15 °C, similarly to the others electrolytes (only the $LiPF_6$ electrolyte shows a higher transition, between -10 °C and 0 °C, during the heating ramp). On the cooling ramp, crystallization occurs in the same temperature range, with the exception of the $LiPF_6$ and LiTDI electrolytes that exhibit larger hysteresis, with delayed crystallizing.

Given the lower dielectric constant (ε (30 °C) = 42.22 [49]) and the higher viscosity of SL, as compared with EC, the conductivity values are lower than their EC:DMC counterparts (LP30 has a conductivity of 10.1 mS cm^{-1} at 20 °C). However, several electrolytes are more conductive than, for instance, the commercial Li-ion electrolyte LP47 (1 M $LiPF_6$ EC:DEC (3:7, wt.)) (σ (20 °C) = 4.6 mS cm^{-1}). The maximum conductivity is reached with LiFSI with 8.15 mS cm^{-1} at 20 °C. It is higher than a 1M LiFSI in pure DMC (8.1 mS cm^{-1} at 25 °C) [50], despite a higher viscosity, showing that SL significantly helps dissociation. LiTFSI and LiDFOB also allow conductivities above 5 mS cm^{-1} at 20 °C. $LiBF_4$ leads to the lowest conductivity values, despite its relatively low induced viscosity. It is in accordance with the low ionic dissociation generally obtained with this salt [2]. On the contrary, the LiTDI electrolyte is more conductive than that incorporating $LiBF_4$ despite its much higher viscosity, which confirms the better dissociation of LiTDI vs $LiBF_4$.

VTF fitting

The viscosity and conductivity curves have been fitted with the VTF equations (2) and (3) to represent the temperature dependency of these electrolytes and the corresponding fitting parameters (η_∞, σ_∞, B, B' T_0, and T_0') are reported in **Table 1**.

$$\eta = \eta_\infty \, e^{\left(\frac{B}{T-T_0}\right)} \qquad \textbf{(2)}$$

$$\sigma = \sigma_\infty \, e^{\left(\frac{-B'}{T-T'_0}\right)} \qquad \textbf{(3)}$$

Table 1. *Van der Waals (VdW) volumes of anions, experimental T_g (taken at the inflection point on the last heating ramp at 5°C min^{-1}) and fitting parameters for the density, conductivity and viscosity.*

	ρ_0 /g cm^{-3}	**a /g cm^{-3} °C^{-1}**	**ln(η_∞ /mPa s)**	**B /K**	**T_0 /K**	**ln(σ_∞ / mS cm^{-1})**	**B' / K**	**T'$_0$ / K**	**VdW Vol. /Å^3**	**Mw /g mol^{-1}**	**T_g /K**
LP30 LiPF$_6$	1.312 ±3.9×10^{-5}	- 0.00116 ±1.1×10^{-6}	-2.231 (-2.285, -2.176)	528.1 (510.9, 545.3)	143.3 (140.8, 145.8)	5.093 (4.852, 5.333)	365.1 (297.1, 433.1)	158.3 (145.4, 171.3)	69 [51]	145.0	193
1 M LiDFOB	1.257 ±2.9×10^{-4}	- 0.00108 ±8.2×10^{-6}	-2.288 (-2.4, -2.175)	600.4 (564.2, 636.6)	139 (134.2, 143.8)	4.411 (4.36, 4.462)	357.4 (343.6, 371.2)	164.5 (162, 167.1)	84 [52]	136.8	186
1 M LiBF$_4$	1.255 ±6.4×10^{-5}	- 0.00101 ±1.8×10^{-6}	-2.41 (-2.466, -2.355)	677.2 (658.1, 696.4)	127.4 (124.9, 129.8)	3.723 (3.14, 4.305)	429.5 (263.9, 595)	148.5 (121.3, 175.6)	49 [51]	86.8	187
1 M LiFSI	1.282 ±6.6×10^{-5}	- 0.00105 ±1.8×10^{-6}	-2.592 (-2.773, -2.412)	736.4 (670.5, 802.3)	117.9 (109.8, 126)	4.612 (4.591, 4.633)	355.7 (349.6, 361.7)	156.7 (155.5, 157.9)	95 [51]	180.1	175

1 M $LiPF_6$	1.284 $\pm 1.9\times10^{-4}$	- 0.00110 $\pm 5.5\times10^{-6}$	-2.342 (-2.395, -2.289)	642.7 (625.2, 660.1)	135.8 (133.6, 138)	4.587 (4.542, 4.632)	363.6 (351.5, 375.7)	162.4 (160.2, 164.6)	69 [51]	145.0	185
1 M LiTFSI	1.317 $\pm 1.1\times10^{-4}$	- 0.00109 $\pm 3.2\times10^{-6}$	-2.378 (-2.456, -2.3)	675.7 (649, 702.4)	129.3 (126, 132.7)	4.315 (4.276, 4.354)	343.5 (332.7, 354.3)	161.6 (159.5, 163.8)	147 [51]	280.1	178
1 M LiTDI	1.235 $\pm 5.4\times10^{-4}$	- 0.00103 $\pm 1.5\times10^{-5}$	-2.352 (-2.431, -2.274)	647.7 (622, 673.3)	137.1 (133.9, 140.3)	4.884 (4.826, 4.941)	517.5 (501.3, 533.8)	152.1 (149.9, 154.3)	134.1 [53]	187.1	190

The values of T_0 and T'_0, are significantly lower than the experimental glass transition temperatures T_g, as it is usually observed [54]. T_0, T'_0 and T_g generally follow the same trend as viscosity. For LiTDI, T_0 and T'_0 are rather low (*i.e.* in the same range as LiTFSI), but the experimental T_g is more in line with its high viscosity.

The Walden plots of the electrolytes are shown in Figure 2d. It is usually considered that the position of the curves defines the *'ionicity'* of solutions lying in the area below the *'ideal KCl line'*. It becomes higher as they are closer to the line [55,56]. Therefore, the '*ionicities'* of the electrolytes are all lower than that of the LP30 electrolyte and follows the same trend as the conductivity values.

Electrochemical stability window (ESW)

Figure 3a shows the electrochemical stability windows of the electrolyte on planar electrodes. The electrolytes seem all stable within 0-5 V vs. Li/Li^+, except the LiTDI electrolyte, and the zoom in reduction shows only minor background reduction currents, in the 5-15 µA cm^{-2} range prior Li plating. In oxidation, the LiTDI electrolyte has the lowest anodic stability, probably due to LiTDI own oxidation. However, the zoom in oxidation (top insert) reveals very low background currents up to 4.5 V for this electrolyte. On the other hand, the other electrolytes extensively oxidize only between 5 and 6 V. However, the insert shows significant background currents prior to the main oxidation currents. For the $LiBF_4$ electrolyte, a peak is observed around

4.5 V and the background current at this voltage is among the highest of all electrolytes, with that of the LiFSI electrolyte. While the currents measured are low, they are likely to play a major role in long term cycling of high voltage electrodes. To emphasize surface reactions and take into account that both Li-ion electrodes usually incorporate conductive carbon (carbon black) of large surface area, which possesses surface groups that might play a role in interfacial reactions and surface passivation, LSVs were also performed with carbon black electrodes on either Cu or Al current collectors and the corresponding voltamperogramms are shown in Figure 3b.

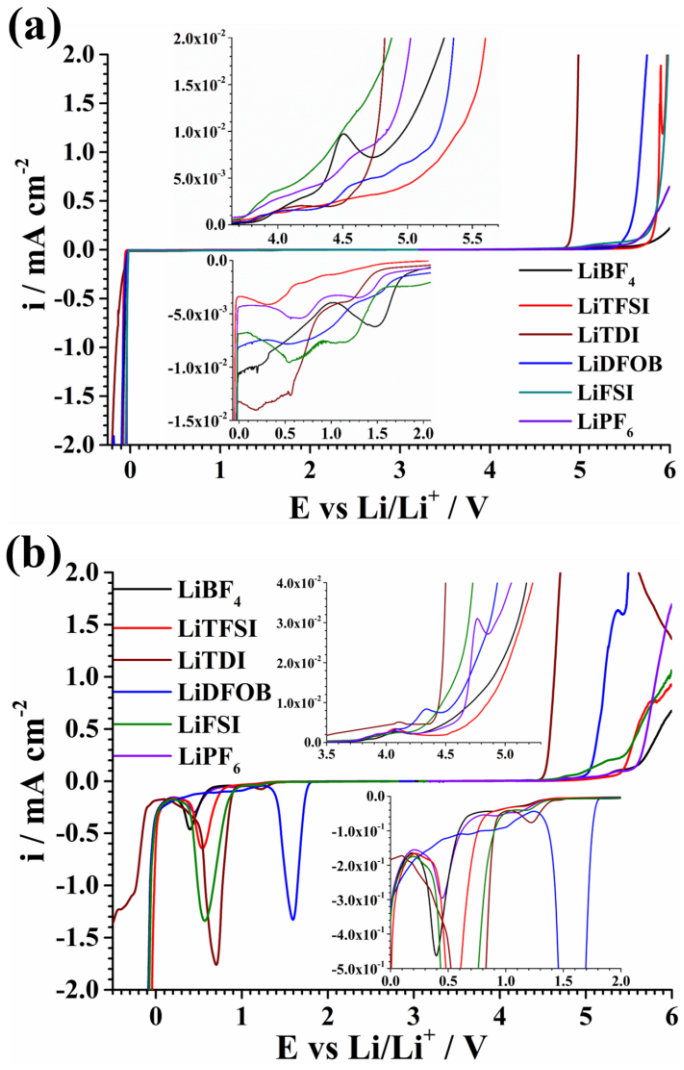

Figure 3 (a) *Linear sweep voltammograms of the 1 M SL:DMC (1:1, wt.) electrolytes. WE: Pt (anodic scan) and Ni (cathodic scan), GF separator, scan rate: 0.1 mV* s^{-1}*. RE and CE: Li.* ***(b)*** *Linear sweep voltammograms of the 1 M SL:DMC (1:1, wt) electrolytes. WE: Super C65 on Al (anodic scan) or on Cu (cathodic scan), GF separator, scan rate: 0.1 mV* s^{-1}*. RE and CE: Li*

LiFSI, in this case, besides LiTDI, exhibits the highest background oxidation current above 4.3 V, probably due to Al corrosion, which has been previously observed with this salt and, in some cases, has been attributed to the presence of halide impurities [51,57,58]. The anodic stability of all electrolytes can be reassessed with more realistic values. The LiDFOB electrolyte starts decomposing slightly before 5.0 V, while the LiTDI electrolyte decomposes at *ca.* 4.5 V. LiTFSI, $LiBF_4$ and $LiPF_6$ electrolytes start exhibiting significant background current around 5.1 V-5.2 V and the oxidation currents then increase significantly at higher voltage: *ca.* 5.4 V for LiTFSI and LiFSI and *ca.* 5.5 V for $LiBF_4$ and $LiPF_6$. Stronger currents, linked to surface reactions, are also observed in reduction. The $LiBF_4$ and $LiPF_6$ electrolyte leads to the smallest reduction peaks. The reduction reactions, for both electrolytes, start at a similar potential as in pure carbonate-based electrolytes (i.e. starting around 0.7-0.8 V vs. Li/Li^+) [36]. For the LiDFOB electrolyte, the peak is much larger and starts around 1.8 V vs. Li/Li^+, which is also similar to what is seen in carbonate-based electrolytes [36]. In this case, the peak has a symmetrical triangular shape that is characteristic of a reduction reaction controlled by the saturation of surface sites. This first reduction process ends at *ca.* 1.2 V and do not overlap much with other reduction processes (such as Li^+ insertion into carbon). The LiTDI electrolyte exhibits a small peak starting at ca. 1.4 V followed by a large symmetrical peak starting at *ca.* 1.0 V. In this case, however, the peak shape is distorted with another reduction process probably starting at *ca.* 0.5 V. For this electrolyte, the lithium deposition is significantly shifted to a lower potential, as compared to the other electrolytes, hinting to a highly resistive SEI for Li^+ transport. The LiFSI electrolyte also exhibits a large peak, starting at a similar voltage as the LiTDI electrolyte and the LiTFSI electrolyte reduction peak starts at *ca.* 0.85 V. This contrasts to what was reported in EC-based electrolytes (with binder-free graphite electrodes), where no obvious differences were observed with $LiPF_6$ and $LiBF_4$ electrolytes [36]. All electrolytes but that with LiTDI allows lithium deposition at *ca.* 0 V.

Performance of graphite electrodes

Figure 4 shows the rate performance of graphite electrodes (7.5 mg cm^{-2}) in half-cell in the SL:DMC electrolytes. With the LiTDI electrolyte (Figure 4b), a rather long reduction plateau is observed at *ca.* 0.8 V

and the ohmic drop at C/10 is very high, even in the first cycle, most likely due to a thick and resistive SEI formed as reported in carbonate mixtures without additives [59] and the capacity drops dramatically with cycling. All the other salts appear to allow graphite electrode operation, although with moderate rate capability. As shown in Figure 4c, for the LiFSI electrolyte, the ohmic drop is not as dramatic as for LiTDI, but the rate performance is very low despite the fact that the electrolyte is the most conductive. The efficiencies are low from the beginning and, as for LiTDI, the capacity decay at C/10 is marked and no capacity can be cycled after the rate-test with this electrolyte. If we compare with $LiBF_4$ (Figure 4e), the less conductive electrolyte, we can see that the $LiBF_4$ electrolyte performs far better with, in particular, well defined insertion plateaus at C/5 and stable capacity, which shows the poor properties of the SEI layers formed in the LiFSI electrolyte (be them on Li metal or graphite), whereas this salt has shown good performance vs. either graphite or Li metal, in either carbonate-based electrolytes [36,60] or in ionic liquids-based electrolytes [61,62]. LiTFSI (Figure 4d) shows decent initial performance with well-defined plateaus until C/5. However, Li^+ transport becomes slower over cycling and the capacity at C/2 decays significantly. $LiPF_6$ (Figure 4f) also shows decent performance up to C/5, as already reported with different graphite electrodes [35]. For this salt as well, the performance decays significantly over cycling, which has been linked with the slow Li^+ transport at the Li metal counter electrode/electrolyte interface [35]. Here, we observe that the performance of $LiPF_6$ is lower than that of LiDFOB (Figure 4g). In fact, most of the electrolytes perform worse than LP47 (Figure 4h), a moderately conductive commercial electrolyte, with the exception of the LiDFOB electrolyte which allows both higher rate capability and stable cycling at C/2.

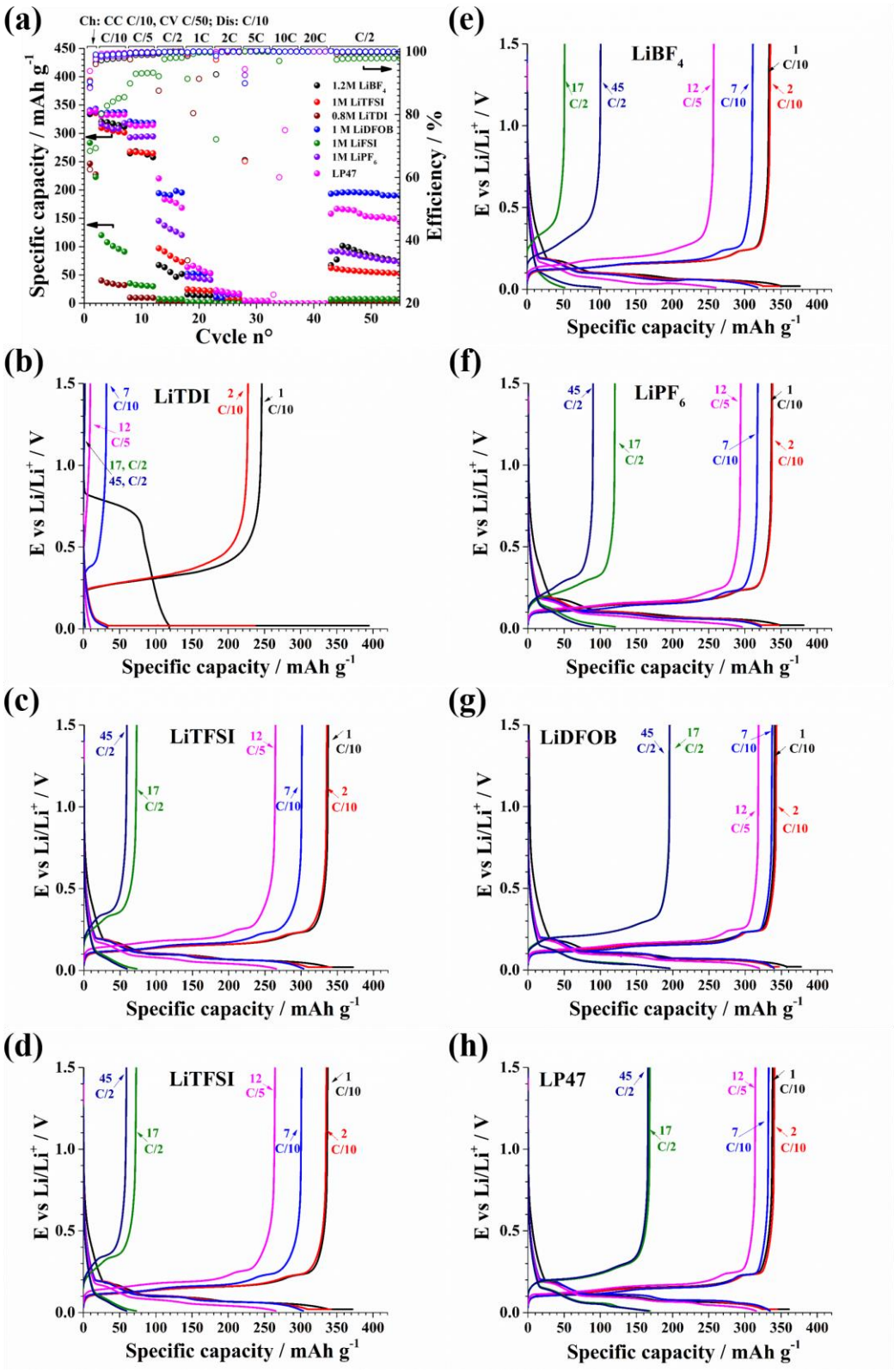

Figure 4. *Rate performance of graphite electrodes in SL:DMC (1:1,wt.) electrolytes.* ***(a)*** *Capacity vs cycle number. Voltage profiles of the electrodes with* ***(b)*** *LiTDI,* ***(c)*** *LiFSI,* ***(d)*** *LiTFSI,* ***(e)*** *$LiBF_4$,* ***(f)*** *$LiPF_6$,* ***(g)*** *LiDFOB,* ***(h)*** *LP47 reference (1M $LiPF_6$ EC/DEC, 3:7)*

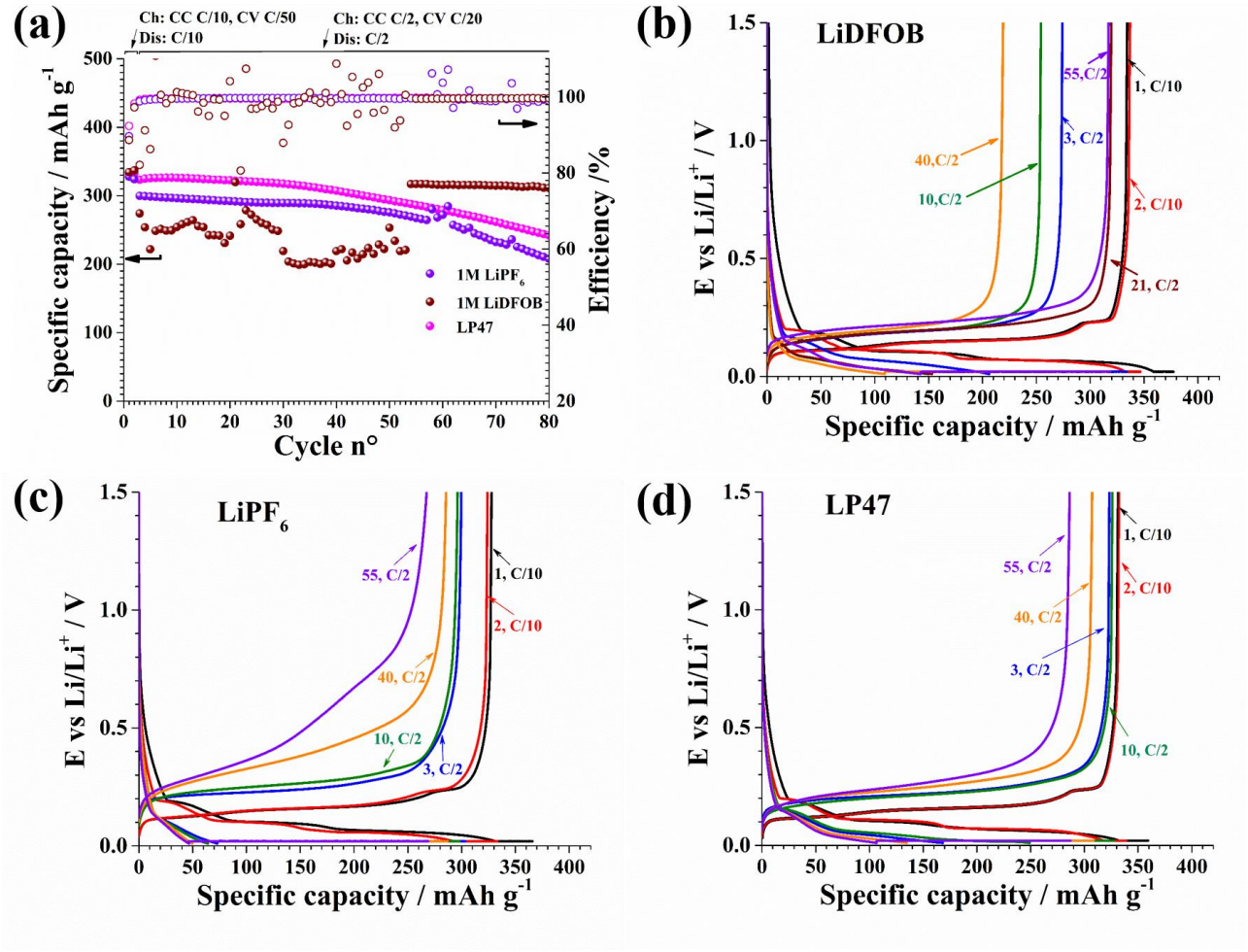

Figure 5. *Cycling performance of graphite electrodes in SL:DMC (1:1,wt.) electrolytes.* ***(a)*** *Capacity and coulombic efficiency vs cycle number. Corresponding (selected) voltage profiles with* ***(b)*** *the LiDFOB electrolyte,* ***(c)*** *the $LiPF_6$ electrolyte and* ***(d)*** *LP47 reference electrolyte.*

Further cycling tests were conducted at constant current with the $LiPF_6$ and LiDFOB electrolytes and the results are shown in Figure 5. In terms of cycling stability, different behaviors can be observed. For the 1 M $LiPF_6$ electrolyte, the capacities are rather stable but the values are inferior to those of LP47. After *ca.* 35 cycles, the two cells with the $LiPF_6$ electrolytes start decaying at a faster rate, probably due to electrolyte consumption. The slopped voltage profiles (shown in Figure 5c) show that the diffusion of Li^+ is becoming significantly slower from cycle 10 to cycle 40 and even more obviously at cycle 55. Even in the first charge at

C/2, the capacity inserted galvanostatically is rather low. On the other hand, as seen Figure 5d, LP47 allows inserting galvanostatically *ca.* 180 mAh g^{-1} in the first cycle and still above 100 mAh g^{-1} in cycle 55.

The 1 M LiDFOB electrolyte exhibits a 'recovery' behavior after *ca.* 55 cycles. It suggests that the issue originates from the Li metal counter electrode, which suddenly starts performing better (*i.e.* the Li metal counter is 'depassivated' by surface rearrangement/dendrites). After around 55 cycles, the capacity becomes very stable and higher than those of the other electrolytes, with also higher efficiencies (above 99.6%). The voltage profiles (shown in Figure 5b) show that the discharge voltage plateau of cycle 40 is much shorter compared with that of cycle 55. It probably means that full areas of the graphite electrode were not accessed (as a result of partial blocking of the Li counter electrode facing them) and are then depassivated during the cycling. Thus, $LiFePO_4$ electrodes were used to substitute the Li metal counter electrode, as a common feature of SL:DMC electrolytes seems to be a poor Li metal counter electrode performance at room temperature.

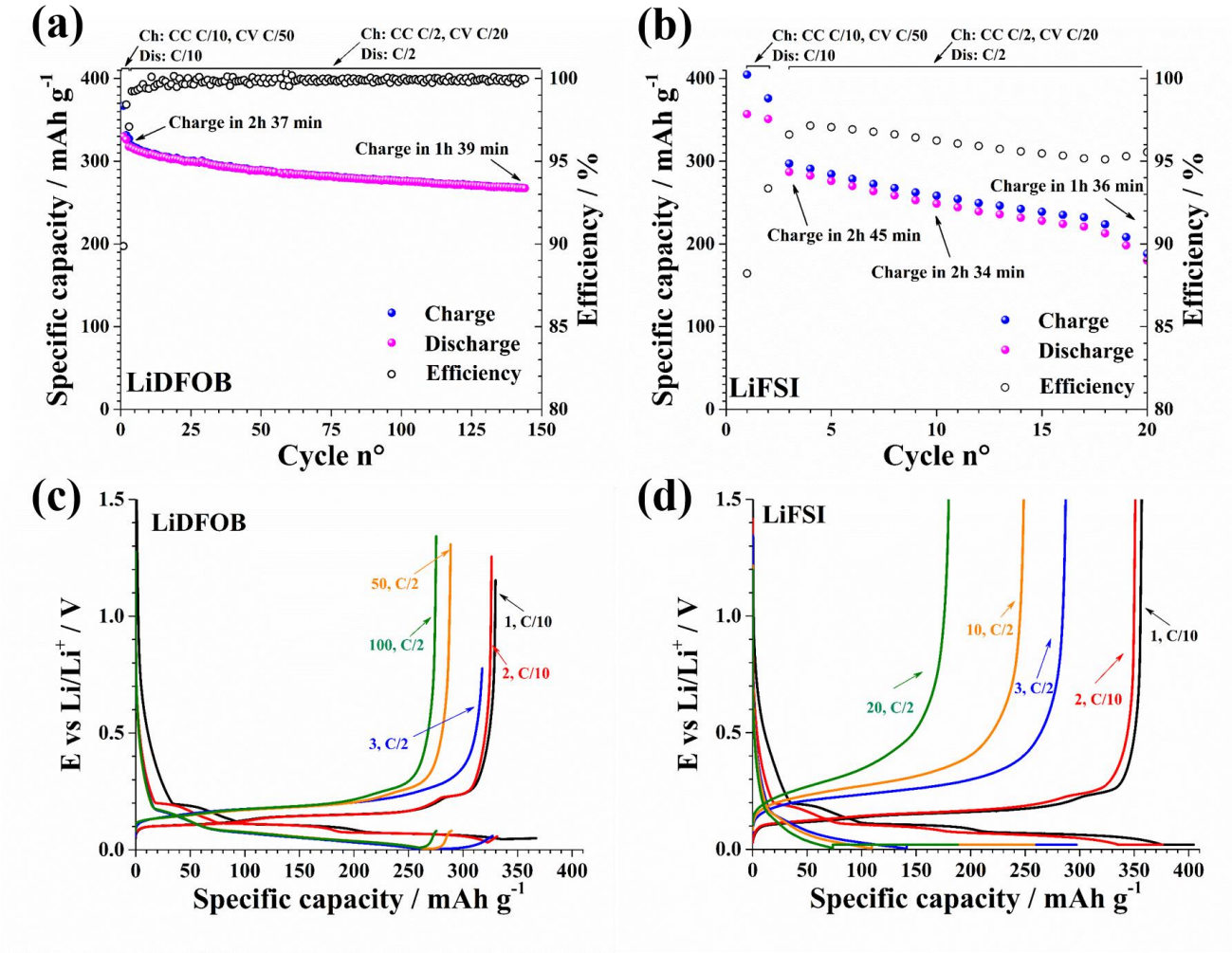

Figure 6. (a) *Capacity and efficiency of a $LiFePO_4$/graphite cell (specific capacity refers to the graphite electrode) in 1 M LiDFOB SL:DMC (1:1,wt.) electrolyte. RE: Li, WE: $LiFePO_4$ (cut-off voltages: 2.0 V-3.5 V) Capacity and performance of a graphite electrode in 1 M LiFSI SL:DMC (1:1,wt.). RE: Li, CE: $LiFePO_4$*

As shown in Figure 6a, the 1 M LiDFOB SL:DMC (1:1, wt.) electrolyte, when lithium is not used as counter electrode, allows efficient and steady cycling of graphite, with efficiencies close to 100% (99.83% average efficiency after the first cycle). The rate performance is significantly improved as most of the insertion occurs during the galvanostatic step at C/2, as shown in Figure 6c, resulting in a full charge in less than 2 h 30 min. On the other hand, the 1 M LiFSI SL:DMC (1:1, wt.) electrolyte, leads to much lower efficiencies (Figure 6b) and, despites its higher conductivity, the graphite electrode is mostly charged during the constant voltage step (Figure 6d), which indicates that the SEI formed on graphite limits the charge. Figure 6c also shows that, for the LiDFOB electrolyte, the insertion voltage profiles are well superimposed from cycle 3 to cycle 100, showing no sign of Li^+ diffusion hindrance by SEI build-up. If we compare these results with the half-cells results, it is clear that Li metal rather than graphite is problematic with the LiDFOB electrolyte. On the other hand, even with a $LiFePO_4$ counter electrode, Figure 6d shows a clear evolution of the potential profiles of the graphite electrode when the LiFSI electrolyte is used, which indicates that the SEI evolves with cycling in accordance with the lower efficiencies and fast capacity decay.

Conclusion

Sulfolane can be used as an EC alternative for cycling graphite-based Li-ion batteries. Without additive, efficiencies around 90% are obtained in the first cycle. Out of $LiBF_4$, $LiPF_6$, LiFSI, LiTFSI, LiDFOB and LiTDI, only LiTDI and, more surprisingly, LiFSI, did not allow graphite electrode cycling in half-cells. LiDFOB even allowed better performance than the EC-based LP47 electrolyte. However, the performances in half-cells are strongly influenced by the Li metal counter electrode. By substituting Li metal with a $LiFePO_4$ counter electrode, it is possible to show improved graphite performance, with efficiency above 90% in the first cycle and above 99.8% in the following cycles with LiDFOB. LiFSI, however, even without Li metal counter electrode, does not form a stable and protective SEI on graphite in SL:DMC. It is likely that the use of well-known additives, such as VC, FEC or LiBOB could help the SEI formation on graphite and lead to further improvements.

Acknowledgements

The research presented is part of the ‘SPICY’ project funded by the European Union’s Horizon 2020 research and innovation program under grant agreement N° 653373

References

[1] J. Tarascon, D. Guyomard, New electrolyte compositions stable over the 0 to 5 V voltage range and compatible with the Li1+xMn2O4/carbon Li-ion cells, Solid State Ionics. 69 (1994) 293–305. doi:10.1016/0167-2738(94)90418-9.

[2] K. Xu, Nonaqueous liquid electrolytes for lithium-based rechargeable batteries, Chem. Rev. 104 (2004) 4303–4417. doi:10.1021/cr030203g.

[3] K. Xu, Electrolytes and Interphases in Li-Ion Batteries and Beyond, Chem. Rev. 114 (2014) 11503–11618. doi:10.1021/cr500003w.

[4] E. Peled, The Electrochemical Behavior of Alkali and Alkaline Earth Metals in Nonaqueous Battery Systems—The Solid Electrolyte Interphase Model, J. Electrochem. Soc. 126 (1979) 2047. doi:10.1149/1.2128859.

[5] J.R. Fong, R. von Sacken U. Dahn, Studies of Lithium Intercalation into Carbons Using Nonaqueous Electrochemical Cells, J. Electrochem. Soc. 137 (1990) 2009–2013. doi:10.1149/1.2086855.

[6] S.K. Jeong, M. Inaba, R. Mogi, Y. Iriyama, T. Abe, Z. Ogumi, Surface film formation on a graphite negative electrode in lithium-ion batteries: Atomic force microscopy study on the effects of film-forming additives in propylene carbonate solutions, Langmuir. 17 (2001) 8281–8286. doi:10.1021/la015553h.

[7] A.J. Gmitter, I. Plitz, G.G. Amatucci, High Concentration Dinitrile, 3-Alkoxypropionitrile, and Linear Carbonate Electrolytes Enabled by Vinylene and Monofluoroethylene Carbonate Additives, J. Electrochem. Soc. 159 (2012) A370. doi:10.1149/2.016204jes.

[8] X. Sun, C.A. Angell, Doped sulfone electrolytes for high voltage Li-ion cell applications, Electrochem. Commun. 11 (2009) 1418–1421. doi:10.1016/j.elecom.2009.05.020.

[9] M. Holzapfel, C. Jost, P. Novák, Stable cycling of graphite in an ionic liquid based electrolyte., Chem. Commun. (Camb). (2004) 2098–2099. doi:10.1039/b407526a.

[10] Q. Zhong, A. Bonakclarpour, M. Zhang, Y. Gao, J.R. Dahn, Synthesis and Electrochemistry of $LiNi_xMn_{2-x}O_4$, J. Electrochem. Soc. 144 (1997) 205–213. doi:10.1149/1.1837386.

[11] R. Santhanam, B. Rambabu, Research progress in high voltage spinel $LiNi_{0.5}Mn_{1.5}O_4$ material, J. Power Sources. 195 (2010) 5442–5451. doi:10.1016/j.jpowsour.2010.03.067.

[12] K. Amine, H. Yasuda, M. Yamachi, Olivine $LiCoPO_4$ as 4.8 V Electrode Material for Lithium Batteries, Electrochem. Solid-State Lett. 3 (1999) 178. doi:10.1149/1.1390994.

[13] S. Brutti, S. Panero, Recent Advances in the Development of $LiCoPO_4$ as High Voltage Cathode Material for Li-Ion Batteries, Nanotechnology for Sustainable Energy. (2013) , 67-99. doi:10.1021/bk-2013-1140.ch004

[14] S. Okada, M. Ueno, Y. Uebou, J.I. Yamaki, Fluoride phosphate Li_2CoPO_4F as a high-voltage cathode in Li-ion batteries, J. Power Sources. 146 (2005) 565–569. doi:10.1016/j.jpowsour.2005.03.149.

[15] X. Wu, Z. Gong, S. Tan, Y. Yang, Sol–gel synthesis of Li_2CoPO_4F/C nanocomposite as a high power cathode material for lithium ion batteries, J. Power Sources. 220 (2012) 122–129. doi:10.1016/j.jpowsour.2012.07.099.

[16] J.-. Y. Benrabah, D., Arnaud, R., Sanchez, Comparative Ab Initio Calculations on Several Salts, Electrochim. Acta. 40 (1995) 2437–2443. doi:10.1016/0013-4686(95)00210-6.

[17] P. Johansson, Intrinsic anion oxidation potentials, J. Phys. Chem. A. 110 (2006) 12077–12080. doi:10.1021/jp0653297.

[18] O. Borodin, W. Behl, T.R. Jow, Oxidative stability and initial decomposition reactions of carbonate, sulfone, and alkyl phosphate-based electrolytes, J. Phys. Chem. C. 117 (2013) 8661–8682. doi:10.1021/jp400527c.

[19] Y. Wang, L. Xing, W. Li, D. Bedrov, Why do sulfone-based electrolytes show stability at high voltages? insight from density functional theory, J. Phys. Chem. Lett. 4 (2013) 3992–3999. doi:10.1021/jz401726p.

[20] A. Abouimrane, I. Belharouak, K. Amine, Sulfone-based electrolytes for high-voltage Li-ion batteries,

Electrochem. Commun. 11 (2009) 1073–1076. doi:10.1016/j.elecom.2009.03.020.

[21] Y. Watanabe, S. Kinoshita, S. Wada, K. Hoshino, H. Morimoto, S. Tobishima, Electrochemical properties and lithium ion solvation behavior of sulfone–ester mixed electrolytes for high-voltage rechargeable lithium cells, J. Power Sources. 179 (2008) 770–779. doi:10.1016/j.jpowsour.2008.01.006.

[22] L. Xing, J. Vatamanu, O. Borodin, G.D. Smith, D. Bedrov, Electrode/electrolyte interface in sulfolane-based electrolytes for Li ion batteries: A molecular dynamics simulation study, J. Phys. Chem. C. 116 (2012) 23871–23881. doi:10.1021/jp3054179.

[23] J. Vatamanu, O. Borodin, G.D. Smith, Molecular Dynamics Simulation Studies of the Structure of a Mixed Carbonate/$LiPF_6$ Electrolyte near Graphite Surface as a Function of Electrode Potential, J. Phys. Chem. C. 116 (2011) 1114–1121. doi:10.1021/jp2101539.

[24] S. Tan, Y.J. Ji, Z.R. Zhang, Y. Yang, Recent Progress in Research on High-Voltage Electrolytes for Lithium-Ion Batteries, ChemPhysChem. 15 (2014) 1956–1969. doi:10.1002/cphc.201402175.

[25] C.A. Xu, K. Angell, High Anodic Stability of a New Electrolyte Solvent: Unsymmetric Noncyclic Aliphatic Sulfone, J. Electrochem. Soc. 145 (1998) L70. doi:10.1149/1.1838419.

[26] K. Xu, C.A. Angell, Sulfone-Based Electrolytes for Lithium-Ion Batteries, J. Electrochem. Soc. 149 (2002) A920. doi:10.1149/1.1483866.

[27] Y. Matsuda, M. Morita, K. Yamada, K. Hirai, Characteristics of Sulfolane-Based Electrolytes for Rechargeable Lithium Batteries, J. Electrochem. Soc. 132 (1985) 2538. doi:10.1149/1.2113619.

[28] A. Brenner, Note on an Organic-Electrolyte Cell with a High Voltage, J. Electrochem. Soc. 118 (1971) 461–462. doi:10.1149/1.2408081.

[29] A. Lewandowski, B. Kurc, A. Swiderska-Mocek, N. Kusa, Graphite|$LiFePO_4$ lithium-ion battery working at the heat engine coolant temperature, J. Power Sources. 266 (2014) 132–137. doi:10.1016/j.jpowsour.2014.04.083.

[30] S. Li, B. Li, X. Xu, X. Shi, Y. Zhao, L. Mao, X. Cui, Electrochemical performances of two kinds of

electrolytes based on lithium bis(oxalate)borate and sulfolane for advanced lithium ion batteries, J. Power Sources. 209 (2012) 295–300. doi:10.1016/j.jpowsour.2012.03.004.

[31] S. Li, Y. Zhao, X. Shi, B. Li, X. Xu, W. Zhao, X. Cui, Effect of sulfolane on the performance of lithium bis(oxalato)borate-based electrolytes for advanced lithium ion batteries, Electrochim. Acta. 65 (2012) 221–227. doi:http://dx.doi.org/10.1016/j.electacta.2012.01.052.

[32] F. Wu, J. Xiang, L. Li, J. Chen, G. Tan, R. Chen, Study of the electrochemical characteristics of sulfonyl isocyanate/sulfone binary electrolytes for use in lithium-ion batteries, J. Power Sources. 202 (2012) 322–331. doi:10.1016/j.jpowsour.2011.11.065.

[33] A. Lewandowski, B. Kurc, I. Stepniak, A. Swiderska-Mocek, Properties of Li-graphite and $LiFePO_4$ electrodes in $LiPF_6$–sulfolane electrolyte, Electrochim. Acta. 56 (2011) 5972–5978. doi:10.1016/j.electacta.2011.04.105.

[34] J. Xia, J.R. Dahn, Improving sulfolane-based electrolyte for high voltage Li-ion cells with electrolyte additives, J. Power Sources. 324 (2016) 704–711. doi:10.1016/j.jpowsour.2016.06.008.

[35] T. Zhang, I. de Meatza, X. Qi, E. Paillard, Enabling steady graphite anode cycling with high voltage, additive-free, sulfolane-based electrolyte: Role of the binder, J. Power Sources. 356 (2017) 97–102. doi:10.1016/j.jpowsour.2017.04.073.

[36] M. Nie, B.L. Lucht, Role of Lithium Salt on Solid Electrolyte Interface (SEI) Formation and Structure in Lithium Ion Batteries, J. Electrochem. Soc. 161 (2014) A1001–A1006. doi:10.1149/2.054406jes.

[37] G. V. Zhuang, K. Xu, T.R. Jow, P.N. Ross, Study of SEI Layer Formed on Graphite Anodes in PC/LiBOB Electrolyte Using IR Spectroscopy, Electrochem. Solid-State Lett. 7 (2004) A224. doi:10.1149/1.1756855.

[38] G. Gebresilassie, S. Grugeon, G. Gachot, M. Armand, S. Laruelle, Electrochimica Acta LiFSI vs . $LiPF_6$ electrolytes in contact with lithiated graphite : Comparing thermal stabilities and identification of specific SEI-reinforcing additives, Electrochim. Acta. 102 (2013) 133–141. doi:10.1016/j.electacta.2013.03.171.

[39] K. Fujii, S. Seki, S. Fukuda, R. Kanzaki, T. Takamuku, Y. Umebayashi, S.I. Ishiguro, Anion conformation of low-viscosity room-temperature ionic liquid 1-ethyl-3-methylimidazolium bis(fluorosulfonyl) imide, J. Phys. Chem. B. 111 (2007) 12829–12833. doi:10.1021/jp074325e.

[40] P. Johansson, S. Gejji, J. Tegenfeldt, J. Lindgren, The imide ion: potential energy surface and geometries, Electrochim. Acta. 43 (1998) 1375–1379. doi:10.1016/S0013-4686(97)10047-0.

[41] D.M. Seo, O. Borodin, S.-D. Han, Q. Ly, P.D. Boyle, W.A. Henderson, Electrolyte Solvation and Ionic Association II. Acetonitrile-Lithium Salt Mixtures: Highly Dissociated Salts, J. Electrochem. Soc. 159 (2012) A553. doi:10.1149/2.jes112264.

[42] S.-D. Han, O. Borodin, D.M. Seo, Z.-B. Zhou, W.A. Henderson, Electrolyte Solvation and Ionic Association: V. Acetonitrile-Lithium Bis(fluorosulfonyl)imide (LiFSI) Mixtures, J. Electrochem. Soc. 161 (2014) A2042–A2053. doi:10.1149/2.0101414jes.

[43] O. Borodin, G.D. Smith, LiTFSI structure and transport in ethylene carbonate from molecular dynamics simulations, J. Phys. Chem. B. 110 (2006) 4971–4977. doi:10.1021/jp056249q.

[44] D.W. McOwen, S.A. Delp, E. Paillard, C. Herriot, S.-D. Han, P.D. Boyle, R.D. Sommer, W.A. Henderson, Anion coordination interactions in solvates with the lithium salts LiDCTA and LiTDI, J. Phys. Chem. C. 118 (2014). doi:10.1021/jp412601x.

[45] J. Chen, K.S. Han, W.A. Henderson, K.C. Lau, M. Vijayakumar, T. Dzwiniel, H. Pan, L.A. Curtiss, J. Xiao, K.T. Mueller, Y. Shao, J. Liu, Restricting the Solubility of Polysulfides in Li-S Batteries Via Electrolyte Salt Selection, Adv. Energy Mater. 6 (2016) 1–6. doi:10.1002/aenm.201600160.

[46] S.-D. Han, O. Borodin, J.L. Allen, D.M. Seo, D.W. McOwen, S.-H. Yun, W.A. Henderson, Electrolyte Solvation and Ionic Association: IV. Acetonitrile-Lithium Difluoro(oxalato)borate (LiDFOB) Mixtures, J. Electrochem. Soc. 160 (2013) A2100–A2110. doi:10.1149/2.094309jes.

[47] J.W. Vaughn, C.F. Hawkins, Physical Properties of Tetrahydrothiophene-1, 1-Dioxide and 3-Methyltetrahydrothiophene-1, 1-Dioxide., J. Chem. Eng. Data. 9 (1964) 140–142. doi:10.1021/je60020a047.

[48] C.L. Berhaut, P. Porion, L. Timperman, G. Schmidt, D. Lemordant, M. Anouti, LiTDI as electrolyte salt for Li-ion batteries: Transport properties in EC/DMC, Electrochim. Acta. 180 (2015) 778–787. doi:10.1016/j.electacta.2015.08.165.

[49] A. Chaudhari, S. Ahire, S.C. Mehrotrac, Dielectric relaxation study of pyridine-water and pyridine-sulfolane mixtures using time domain reflectometry, J. Mol. Liq. 94 (2001) 17–25. doi:10.1016/S0167-7322(01)00238-0.

[50] L. Li, S. Zhou, H. Han, H. Li, J. Nie, M. Armand, Z. Zhou, X. Huang, Transport and Electrochemical Properties and Spectral Features of Non-Aqueous Electrolytes Containing LiFSI in Linear Carbonate Solvents, (2011) 74–82. doi:10.1149/1.3514705.

[51] H.B. Han, S.S. Zhou, D.J. Zhang, S.W. Feng, L.F. Li, K. Liu, W.F. Feng, J. Nie, H. Li, X.J. Huang, M. Armand, Z. Bin Zhou, Lithium bis(fluorosulfonyl)imide (LiFSI) as conducting salt for nonaqueous liquid electrolytes for lithium-ion batteries: Physicochemical and electrochemical properties, J. Power Sources. 196 (2011) 3623–3632. doi:10.1016/j.jpowsour.2010.12.040.

[52] N. Nambu, R. Takashi, K. Suzuki, Y. Sasaki, Electrolytic Properties of Tetramethylammonium Compound in Highly Concentrated Solutions and Its Application to Electric Double-Layer Capacitors, Electrochemistry. 81 (2013) 811–813. doi:10.5796/electrochemistry.81.811.

[53] Y.H. Zhao, M.H. Abraham, A.M. Zissimos, Fast Calculation of van der Waals Volume as a Sum of Atomic and Bond Contributions and Its Application to Drug Compounds, J. Org. Chem. 68 (2003) 7368–7373. doi:10.1021/jo034808o.

[54] P.E. Stallworth, J.J. Fontanella, M.C. Wintersgill, C.D. Scheidler, J.J. Immel, S.G. Greenbaum, A.S. Gozdz, NMR, DSC and high pressure electrical conductivity studies of liquid and hybrid electrolytes, J. Power Sources. 81–82 (1999) 739–747. doi:10.1016/S0378-7753(99)00144-5.

[55] E.I. Cooper, C.A. Angell, Ambient temperature plastic crystal fast ion conductors (PLICFICS), Solid State Ionics. 19 (1986) 570–576. doi:10.1016/0167-2738(86)90180-3.

[56] C.A. Angell, (Invited) Ionic Liquids, Superionic Glasses, Quasi-Ionic Liquids, Quasi-Liquid Ionics,

All with High Conductivities but Some with Little Fluidity. Where does the Paradigm End?, ECS Trans. 64 (2014) 9–20. doi:10.1149/06404.0009ecst.

[57] A. Abouimrane, J. Ding, I.J. Davidson, Liquid electrolyte based on lithium bis-fluorosulfonyl imide salt: Aluminum corrosion studies and lithium ion battery investigations, J. Power Sources. 189 (2009) 693–696. doi:10.1016/j.jpowsour.2008.08.077.

[58] M. Kerner, N. Plylahan, J. Scheers, P. Johansson, Thermal stability and decomposition of lithium bis(fluorosulfonyl)imide (LiFSI) salts, RSC Adv. 6 (2016) 23327–23334. doi:10.1039/C5RA25048J.

[59] I.A. Shkrob, K.Z. Pupek, J.A. Gilbert, S.E. Trask, D.P. Abraham, Chemical Stability of Lithium 2-Trifluoromethyl-4,5-dicyanoimidazolide, an Electrolyte Salt for Li-Ion Cells, J. Phys. Chem. C. 120 (2016) 28463–28471. doi:10.1021/acs.jpcc.6b09837.

[60] L. Li, S. Zhou, H. Han, H. Li, J. Nie, M. Armand, Z. Zhou, X. Huang, Transport and Electrochemical Properties and Spectral Features of Non-Aqueous Electrolytes Containing LiFSI in Linear Carbonate Solvents, J. Electrochem. Soc. 158 (2011) A74. doi:10.1149/1.3514705.

[61] M. Ishikawa, T. Sugimoto, M. Kikuta, E. Ishiko, M. Kono, Pure ionic liquid electrolytes compatible with a graphitized carbon negative electrode in rechargeable lithium-ion batteries, 162 (2006) 658–662. doi:10.1016/j.jpowsour.2006.02.077.

[62] E. Paillard, Q. Zhou, W.A. Henderson, G.B. Appetecchi, M. Montanino, S. Passerini, Electrochemical and Physicochemical Properties of PY_{14} FSI-Based Electrolytes with LiFSI, J. Electrochem. Soc. 156 (2009) 891–895. doi:10.1149/1.3208048.